

# A complete quantum description of an ultrafast pump-probe charge transfer event in condensed phase

Christiane P. Koch and Thorsten Klüner

*Fritz-Haber-Institut der Max-Planck-Gesellschaft, Faradayweg 4-6, 14195 Berlin, Germany*

Ronnie Kosloff

*Department of Physical Chemistry and The Fritz Haber Research Center, The Hebrew University, Jerusalem 91904, Israel*

(Received 1 August 2001; accepted 18 December 2001)

An ultrafast photoinduced charge transfer event in condensed phase is simulated. The interaction with the field is treated explicitly within a time-dependent framework. The description of the interaction of the system with its environment is based on the surrogate Hamiltonian method where the infinite number of degrees of freedom of the environment is approximated by a finite set of two-level modes for a limited time. This method is well suited to ultrafast events, since it is not limited by weak coupling between system and environment. Moreover, the influence of the external field on the system-bath coupling is included naturally. The surrogate Hamiltonian method is generalized to incorporate two electronic states including all possible system-bath interactions. The method is applied to a description of a pump-probe experiment where every step of the cycle is treated consistently. Dynamical variables are considered which go beyond rates of charge transfer such as the transient absorption spectrum. The parameters of the model are chosen to mimic the mixed valence system  $(\text{NH}_3)_5\text{RuNCRu}(\text{CN})_5^-$ . © 2002 American Institute of Physics.

[DOI: 10.1063/1.1450124]

## I. INTRODUCTION

Charge transfer reactions in solution have been an ongoing topic of research which continues to draw significant attention.<sup>1</sup> Important examples range from photosynthesis<sup>2,3</sup> to surface photochemistry.<sup>4,5</sup> From the beginning it was clear<sup>6,7</sup> that the environment plays a very important role in determining the fate of the reaction. The shift in charge distribution during the reaction forces a complete rearrangement of the solvation shell. But the environment has an additional important consequence for it forces the dynamics to relax to a kinetic description. The actual act of charge transfer is a dynamical nonadiabatic quantum event. The decoherence caused by the solvent eventually forces the system to localize onto a particular charged state. This localization marks the qualitative change from a dynamical to a kinetic picture. For weak to moderate system-bath coupling, an increase in the dissipative forces will cause an increase in the rate of charge transfer. A further increase in the system-bath coupling will cause a turnover and the rate will decrease.<sup>8</sup> This general quantum phenomenon has been termed the quantum anti-Zeno effect.<sup>9</sup>

New light on the charge transfer process has come from ultrafast pump-probe experiments.<sup>10,11</sup> This technique constitutes a dynamical probe enabling the unraveling of the sequence of events that lead eventually to the charge transfer product. A direct signature of the ultrafast dynamics are transient modulations of optical observables reflecting the promotion of ground and excited state vibrational modes.

The present study is aimed at constructing a comprehensive quantum dynamical model which can describe consistently the experimental observations. The model is built from

a primary system described by a time-dependent wave packet picture. This allows an explicit incorporation of the pulsed radiation as a time-dependent field. The bath is described implicitly with the idea that only its influence on the primary system is important. The infinite number of true bath modes is replaced by a finite number of representative modes which are sufficient to faithfully describe the dynamics for a finite interval of time. The energy interval between these representative modes decreases with  $\hbar/\text{total propagation time}$ . This system-bath scheme has been termed the surrogate Hamiltonian method.<sup>12,13</sup>

The purpose of the present study is to follow the sequence of events from light induced excitation to nonadiabatic transition, and deexcitation back to the ground initial state (cf. Fig. 1). The justification for the use of the surrogate Hamiltonian method is the ultrafast nature of the observations which restrict the time scale. The main goal in the study is to construct a comprehensive model which is able to simulate transient as well as static experimental observables. Special attention is devoted to checking the numerical convergence. Once the calculation has been converged the observations and insight can be attributed to the model.

Direct insight into the complex charge transfer process can be obtained by following the sequence of events (cf. Fig. 1). In general, one can identify four major dissipative processes taking place. The most studied is vibrational relaxation which means the gain/loss of vibrational energy from/to the bath. Electronic quenching is a similar process in which electronic energy is lost to the bath. More subtle are nuclear and electronic dephasing processes. These processes are characterized by loss of either a nuclear phase or an

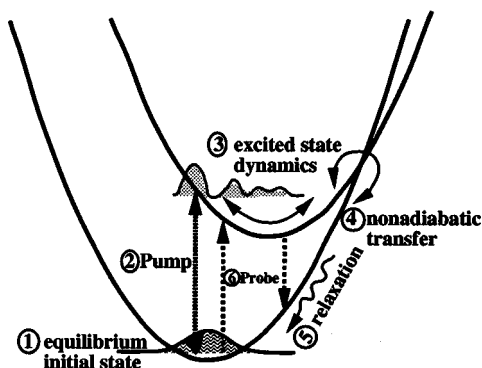


FIG. 1. An excitation-deexcitation cycle. An initial correlated state (1) is partially promoted to the excited electronic state by the pump pulse (2), leaving a “hole” in the ground state density. The excited state population moves to the crossing point (3) where it can cross back to the ground state potential via a nonadiabatic transition (4). Once on the ground electronic surface the hot vibration cools back to the bottom of the well (5). The dynamics is followed in time by a short and weak probe pulse (6).

electronic phase limiting therefore coherent quantum processes. A brief description of the main theoretical considerations for each of the above steps is presented.

- (1) The initial state of the process is a strongly solvated chromophore which results in a system and bath which are highly correlated. The surrogate Hamiltonian method addresses this issue by constructing a correlated initial state which is consistent with the system-bath model (cf. Sec. IV A). This phenomenon is related to nuclear relaxation. The initial correlation has been a major concern for quantum treatments of system-bath dynamics. The common approach is to approximate the initial state as a tensor product between the system and the bath state. A correction to the problem within the context of a perturbative treatment of the system-bath coupling has recently been suggested.<sup>14</sup> This issue has been tested within the current context (cf. Sec. IV B) showing only a small effect on the dynamics.
- (2) The excitation by the pump pulse is the second step in the sequence of events. In most cases the pump intensity is sufficient to promote a significant fraction of the population to the excited state (cf. Sec. IV C). The void or “hole” left on the ground electronic state creates a nonstationary density which then oscillates periodically with the ground state vibrational frequencies.<sup>15,16</sup> This phenomenon is known experimentally as resonance impulsive stimulated Raman scattering (RISRS). The creation of this “hole” can be explained by Rabi cycling which is coordinate dependent. This means that a consistent description of the excitation process has to include explicitly the interaction with the radiation. Moreover, the strong interaction with the field has been shown to modify the system-bath coupling.<sup>17–19</sup> For charge transfer events in solution the time scale of electronic dephasing is of the same order as the pulse duration forcing a description which includes explicitly this phenomenon. Another effect is due to an interference between the radiation induced excitation and back transfer caused by the diabatic coupling. If the diabatic coupling potential is

not localized on the crossing point, this effect is significant (cf. Sec. IV C). The explicit time dependence in the surrogate Hamiltonian theory is designed to include these effects within the model. The state of the system has to reflect the full nonadiabatic picture thus having amplitude on the two potential energy surfaces simultaneously. This is in contrast to the common perturbation theory picture which places the ground state wave packet on the excited electronic surface.<sup>8</sup>

- (3) Once the excitation has promoted population to the excited electronic surface, the excited state wave function starts to evolve, eventually reaching the crossing point. This evolution is also strongly influenced by the bath. Strong vibrational relaxation on the excited state can stop the motion before it reaches the crossing point (cf. Sec. IV E). The nonstationary “hole” left on the ground electronic surface will also start to evolve, causing periodic modulations with frequencies characteristic of Raman transitions.<sup>16</sup> The decay of these modulations is influenced by vibrational dephasing and relaxation.
- (4) The density approaching the crossing point can cross by nonadiabatic charge transfer back to the ground electronic potential. This step is crucially influenced by the environment. The dynamics has to reflect the turnover from an enhancement of the charge transfer rate caused by an increase in dissipation to a suppression of the rate. The difficulty in analyzing this step is that it is influenced by all the dissipative processes.
- (5) Following the charge transfer event, the vibrational modes on the ground electronic state are highly excited. If the time scale of the charge transfer event is fast relative to a vibrational period, the new wave packet will have coherent properties. The final stage in closing the cycle of events is the recovery of the initial equilibrium state. This is the result of vibrational relaxation of the excess energy to the bath (cf. Sec. IV D).
- (6) The probe pulse can be applied at any stage in the cycle of events. Typically, the probe pulse is short and weak. It can promote both an excitation, which means absorption of energy, or deexcitation, resulting in stimulated emission. In this case a perturbative picture is justified and can save significant computational effort. This viewpoint leads to the concept of a window operator which describes the total energy balance absorbed or emitted from the probe pulse (cf. Sec. IID 2).

The present study is aimed at developing the methodological tools for modeling ultrafast dynamics in a dissipative environment. The sequence of events above is typical and can supply the main insight required.

The article is organized as follows: Section II reviews the surrogate Hamiltonian method, introduces the basic charge transfer model and makes the connection to observables. The dissipative processes and their treatment within the surrogate Hamiltonian are described in Sec. III, in particular dephasing is introduced in Sec. III B. The results are presented in Sec. IV, while Sec. V concludes the study.

## II. THE SURROGATE HAMILTONIAN METHOD

### A. Brief review of the surrogate Hamiltonian

The model to be constructed has to describe a primary system immersed in a bath. The state of the combined system-bath is described by the wave function  $\Psi(Q, \alpha, \sigma_1, \sigma_2, \dots, \sigma_N)$  where  $Q$  represents the nuclear configuration of the dynamical system,  $\alpha$  the electronic level, and  $\sigma_i$  the bath degrees of freedom. The Hamiltonian of such a combined system is

$$\hat{H} = \hat{H}_S + \hat{H}_{SF} + \hat{H}_{SB} + \hat{H}_B \quad (1)$$

with  $\hat{H}_S$  the Hamiltonian of the system,  $\hat{H}_{SF} = \hat{H}_{SF}(t)$  describing the time-dependent interaction of the system with the field,  $\hat{H}_{SB}$  describing the interaction of the system with the bath and  $\hat{H}_B$  the bath Hamiltonian. The observables are associated with operators of the primary system. They are determined from the reduced system density operator:  $\hat{\rho}_S(Q, Q') = \text{tr}_B\{|\Psi\rangle\langle\Psi|\}$ , where  $\text{tr}_B\{\}$  is a partial trace over the bath degrees of freedom, i.e., the system density operator is constructed from the total system-bath wave function while only this wave function is propagated.

The computational requirements in a quantum mechanical simulation scale exponentially with the number of degrees of freedom. Therefore some drastic reduction of complexity is needed. The primary system is to be represented in full quantum rigor which includes two potential energy surfaces, and the relevant nuclear configurations. A grid representation is used in this study to represent the wave function on each surface. This primary system is different from previous applications of the surrogate Hamiltonian method where only ground state dynamics was considered.<sup>12,13,20</sup>

The main reduction in complexity is in the construction of the bath. The infinite number of bath modes is to be replaced by a finite number of representative modes. Since within a finite interval of time, the system cannot resolve the full density of states of the bath, it is sufficient to replace the bath modes by a finite set. The sampling density in energy of this set is determined by the inverse of the time interval.

There are two general classes of commonly used bath descriptions. The first is a bath composed of harmonic oscillators. The second class is a bath composed from a set of two-level systems (TLSs).<sup>21</sup> The idea of a harmonic bath originates from a normal mode analysis combined with a weak system-bath coupling which guarantees that the harmonic approximation is valid. A spin bath can be thought of as originating from a prediagonalization of the bath to its energy levels. It then represents the energy spectrum by a set of two-level systems.

The harmonic bath has been the starting point of many system-bath studies which are based on either path integrals or semiclassical approximations.<sup>22–25</sup> The harmonic bath's influence on the system is completely specified by the spectral density function  $J(\epsilon)$  which is determined by the density of states weighted by the coupling. The similarity between classical and quantum harmonic baths is the source of a method of obtaining the spectral density from classical MD simulations of the bath.<sup>26</sup>

The spin bath is harder to construct,<sup>21</sup> but for sufficiently low temperature it coincides with the harmonic bath. For higher temperature the parameters of the spin bath can be obtained by a scaling term which is applied to the spectral density of the harmonic bath:<sup>21,23–25</sup>

$$J_{\text{osc}}(\omega) = \tanh\left(\frac{1}{2}\hbar\omega\beta\right)J_{\text{spin}}(\omega) \quad (2)$$

with  $\beta = 1/k_B T$ . This procedure is employed whenever one compares to a harmonic bath.

### B. The basic charge transfer model

The system Hamiltonian is constructed from the nuclear configurations on two electronic states in a diabatic representation:

$$\hat{H}_S = \begin{pmatrix} \hat{H}_g & V_d(\hat{Q}) \\ V_d(\hat{Q}) & \hat{H}_e \end{pmatrix} \otimes \mathbb{1}_B \quad (3)$$

with  $\hat{H}_{g/e} = \hat{T} + V_{g/e}(\hat{Q})$ .  $\hat{T} = \hat{P}^2/2M$  is the kinetic energy operator,  $V_g$  and  $V_e$  are the potential energy operators of the electronic ground and excited state, and  $V_d$  is the diabatic coupling.

The coupling with radiation is described by the time-dependent Hamiltonian

$$\hat{H}_{SF} = \begin{pmatrix} 0 & -E(t)\hat{\mu}_{tr} \\ -E^*(t)\hat{\mu}_{tr} & 0 \end{pmatrix} \otimes \mathbb{1}_B, \quad (4)$$

where  $\hat{\mu}_{tr} = \hat{\mu}_{tr}(\hat{Q})$  is the transition dipole operator which can be a function of the nuclear configuration.  $E(t)$  is the time-dependent electric field, and by employing the long wavelength approximation, the spatial dependence of  $E(t)$  is ignored.

Finally, the surrogate bath Hamiltonian has the form

$$\hat{H}_B = \mathbb{1}_S \otimes \sum_i \varepsilon_i \hat{\sigma}_i^\dagger \hat{\sigma}_i, \quad (5)$$

where  $\varepsilon_i$  are the representative energy eigenvalues, and  $\hat{\sigma}_i^\dagger \hat{\sigma}_i$  are the creation and annihilation operators of the representative mode  $i$ . More than one effective bath can be employed, each related to a different dissipative phenomenon. The interaction of system and bath is described by the Hamiltonian  $\hat{H}_{SB}$ . This operator will be discussed in detail in Sec. III.

### C. Numerical implementation

The state of the system combined with the bath is described by a  $2^N$ -dimensional spinor with  $N$  being the number of modes. For  $N=1$  it becomes

$$\Psi(\hat{Q}) = \begin{pmatrix} \psi_0(\hat{Q}, \alpha) \\ \psi_1(\hat{Q}, \alpha) \end{pmatrix}, \quad (6)$$

where  $\hat{Q}$  represents the nuclear degrees of freedom of the wave function and  $\alpha$  the electronic degrees of freedom. The spinor is bit ordered, i.e., the  $i$ th bit set in the spinor index corresponds to the  $i$ th TLS mode excited if the counting of bits starts at  $i=0$ . The number of simultaneous excitations can be restricted. The dimension of the spinor is then given

by the sum of binomial coefficients  $\sum_{i=0}^{N_{\text{exc}}} \binom{N_{\text{exc}}}{i}$  with  $N_{\text{exc}}$  the number of simultaneously allowed excitations.

The dynamics of the system combined with the bath is generated by solving the time-dependent Schrödinger equation:

$$\Psi(\hat{\mathbf{Q}}; t) = e^{-i\hat{\mathbf{H}}t} \Psi(\hat{\mathbf{Q}}; 0). \quad (7)$$

Each spinor component  $\psi_i(\hat{\mathbf{Q}})$  is represented on a spatial grid describing the nuclear configurations. The kinetic energy operator is applied in Fourier space employing FFTs,<sup>27</sup> and the Chebychev method<sup>28</sup> is used to compute the evolution operator.

For  $N$  modes the representation of the  $i$ th bath operator is

$$\hat{\sigma}_i^\dagger = \prod_{j=1}^{N-i} \mathbb{1}_2 \otimes \hat{\sigma}_i^\dagger \otimes \prod_{j=1}^{i-1} \mathbb{1}_2 \quad (8)$$

with

$$\hat{\sigma}_i^\dagger = \begin{pmatrix} 0 & 0 \\ 1 & 0 \end{pmatrix}. \quad (9)$$

The matrix representation of  $\sum_i d_i (\hat{\sigma}_i^\dagger + \hat{\sigma}_i)$  has already been given.<sup>12</sup> In the bit representation, the operator  $\sum_{ij} c_{ij} (\hat{\sigma}_i^\dagger \hat{\sigma}_j + \hat{\sigma}_j^\dagger \hat{\sigma}_i)$  for  $N=3$  modes corresponds to

$$\sum_{i,j=1}^3 c_{ij} (\hat{\sigma}_i^\dagger \hat{\sigma}_j + \hat{\sigma}_j^\dagger \hat{\sigma}_i) = \begin{pmatrix} 0 & 0 & 0 & 0 & 0 & 0 & 0 & 0 \\ 0 & 0 & c_{12} & 0 & c_{13} & 0 & 0 & 0 \\ 0 & c_{21} & 0 & 0 & c_{23} & 0 & 0 & 0 \\ 0 & 0 & 0 & 0 & 0 & c_{23} & c_{13} & 0 \\ 0 & c_{31} & c_{32} & 0 & 0 & 0 & 0 & 0 \\ 0 & 0 & 0 & c_{32} & 0 & 0 & c_{12} & 0 \\ 0 & 0 & 0 & c_{31} & 0 & c_{21} & 0 & 0 \\ 0 & 0 & 0 & 0 & 0 & 0 & 0 & 0 \end{pmatrix}. \quad (10)$$

These matrices do not have to be stored but can be more efficiently applied by bit-testing. To apply the bath Hamiltonian [Eq. (5)], the  $k$ th spinor component is multiplied with the bath energy  $\varepsilon_i$  if the  $i$ th bit in  $k$  is set. The action of the bath operators  $\sum_i d_i (\hat{\sigma}_i^\dagger + \hat{\sigma}_i)$  is given by an exclusive *or*. That is, if  $k = \text{EOR}(2^i, l)$ , then  $d_i \psi_l(Q)$  needs to be added to the  $k$ th component of the new spinor. The application of Eq. (10) requires several bit tests: First, the number of excitations in the indices  $k$  and  $l$  must be equal and, second, the indices of  $c_{ij}$  in Eq. (10) numbering the bath modes (not the spinor components) bit-added,  $i+j$ , must be equal to the exclusive *or* of  $k$  and  $l$ .

From Eq. (10) it can be seen that there is no pure dephasing for a bath at zero temperature: At zero temperature no TLS is excited corresponding to all population being in the 0th spinor component. Furthermore, dephasing cannot create bath excitations, i.e., it operates only between spinor components with the same number of excitations.

## D. Observables and data analysis

Most observables of interest can be obtained as expectation values of system operators. The system's state is constructed by a Boltzmann average of a trace over the bath of the total wave function:

$$\hat{\rho}_s(t) = \text{tr}_B \{ \hat{\mathbf{U}}(t) |\Psi(0)\rangle \langle \Psi(0)| \hat{\mathbf{U}}^\dagger(t) \} \quad (11)$$

with  $|\Psi(0)\rangle \langle \Psi(0)| = \sum_j (e^{-\beta E_j} / Z) |\Psi_j\rangle \langle \Psi_j|$ , where  $\beta = 1/k_b T$  and  $Z = \sum_j e^{-\beta E_j}$ .  $E_j$  is the energy of the  $j$ th eigenfunction  $|\Psi_j\rangle$ . The initial condition for the wave function  $|\Psi(0)\rangle$  is obtained by calculating the lowest energy eigenfunctions of the combined system-bath Hamiltonian.

### 1. Power absorption

For the radiation, a time-dependent semiclassical approximation is used. The power absorbed or emitted from the radiation field is then given by the expectation value:<sup>29</sup>

$$\mathcal{P} = \left\langle \frac{\partial \hat{\mathbf{H}}_{SF}}{\partial t} \right\rangle = \text{tr}_S \left\{ \hat{\rho}_s \frac{\partial \hat{\mathbf{H}}_{SF}}{\partial t} \right\}. \quad (12)$$

To obtain the total energy absorbed by a pulse, Eq. (12) is integrated for the total pulse duration. When the radiation field is represented by a rotating field,  $E(t) = \bar{\varepsilon} e^{i\omega_L t}$ , one obtains

$$\Delta E = \int \mathcal{P} dt = -\hbar \omega_L \Delta N_g. \quad (13)$$

Equation (13) allows association of the change in population from the ground to the excited electronic state,  $\Delta N_g$ , to the energy absorbed from the field.

### 2. Window operator and transient absorption/emission

Despite the option of direct simulation, it is beneficial to employ perturbation theory and represent the total absorption from the probe pulse by an observable represented by a window operator  $\hat{\mathbf{W}}$ . This operator describes a finite resolution position measurement.<sup>30,31</sup>

$$\Delta E \approx -\hbar \omega_L \text{tr}_S \{ \hat{\rho}_s(t_p) \cdot \hat{\mathbf{W}} \}. \quad (14)$$

The observation process is completed in a time duration proportional to the probe pulse duration  $\tau_p$ . The concept of Eq. (14) is to collapse the observation to a single instant of time  $t_p$ . By employing time-dependent perturbation theory the window operator for a Gaussian shaped probe pulse with the envelope function  $\bar{\varepsilon}(t) = A e^{-(t-t_p)^2/2\tau_p^2}$  becomes<sup>30,31</sup>

$$\hat{\mathbf{W}}(\hat{\mathbf{Q}}, \hat{\mathbf{Q}}') = \frac{\pi(\tau_p A)^2}{\hbar^2} e^{-2\Delta(\hat{\mathbf{Q}})^2/\hbar^2 \tau_p^2} \cdot \hat{\mu}^2(\hat{\mathbf{Q}}) \times \delta(\hat{\mathbf{Q}} - \hat{\mathbf{Q}}') |\alpha\rangle \langle \alpha|, \quad (15)$$

where  $|\alpha\rangle \langle \alpha|$  is the electronic projection operator which selects the ground electronic state for transient absorption. For emission, the projection operator selects the excited electronic state. The window operator, Eq. (15), is a function of the probe central frequency  $\omega_L$ :

$$2\Delta(\hat{\mathbf{Q}}) = V_e(\hat{\mathbf{Q}}) - V_g(\hat{\mathbf{Q}}) - \hbar \omega_L, \quad (16)$$

i.e.,  $2\Delta(\hat{Q})$  is the difference potential. The employment of the window operator is based on the assumption of a random phase between the pump and probe pulses, so that interference effects will be eliminated. Interference between pump and probe signals is also eliminated once electronic dissipation is complete. The memory of the pump phase is stored in the transition dipole phase. This is erased once the relative phase between the ground and excited state wave packets is lost by electronic dephasing.<sup>32</sup>

### 3. Correlation functions

The theory of linear response associates the weak field spectral response of matter to Fourier transforms of time correlation functions. These are calculated using the system and bath Hamiltonian without the external field. For example, the CW absorption spectrum is calculated by the following autocorrelation function:<sup>16</sup>

$$C(t) = \langle \Psi_i | \hat{M}(t) | \Psi_i \rangle, \quad (17)$$

where  $|\Psi_i\rangle$  is the initial state. The time-dependent propagator  $\hat{M}$  is defined as

$$\hat{M}(t) = \hat{\mu}_{tr} \{ e^{-i(\hat{H}_S + \hat{H}_{SB} + \hat{H}_B)t} \} \hat{\mu}_{tr} \quad (18)$$

with  $\hat{\mu}_{tr}$  being the transition dipole operator and  $\Psi_i$  the initial stationary state. For finite temperature, a Boltzmann weighted sum over all populated stationary states needs to be considered in Eq. (17). The absorption cross section  $\sigma_A(\omega_L)$  is related to the Fourier transform of the autocorrelation function of the initial state:<sup>33</sup>

$$\sigma_A(\omega_L) \propto \omega_L \text{Im} \left( \int_0^\infty e^{i(\omega_L + \epsilon_i)t} C(t) dt \right), \quad (19)$$

where  $\epsilon_i$  is the energy of the initial state  $\Psi_i$ .

The Raman cross section can be obtained from the half Fourier transform of the correlation function:

$$C_{ji}(t) = \langle \Psi_j | \hat{M}(t) | \Psi_i \rangle, \quad (20)$$

where  $\Psi_j$  is the final wave function.<sup>34</sup>

The method can be extended to treat dispersed fluorescence and gated fluorescence.<sup>35</sup>

### 4. Filter diagonalization

The convergence of the surrogate Hamiltonian method is significantly faster for short propagation times. In order to obtain long time observables or frequency domain results which depend on them, the short-time observables have to be extrapolated. The filter diagonalization technique<sup>36-39</sup> fits the short-time time-series to a model which then can be extrapolated. The method is based on the assumption that the time signal can be represented as a sum of complex exponentials:

$$S(t) = \sum_{j=1}^K d_j \exp(-i\omega_j t), \quad (21)$$

where  $\Omega_j = \text{Re}(\omega_j)$  is the desired frequency,  $\tau_j = 1/\text{Im}(\omega_j)$  is the decay rate and  $d_j$  is the complex amplitude. The number of real fitting parameters is  $4K$ . The parameters specifying the accuracy of the filter diagonalization method are the

smallest allowed eigenvalue of the overlap matrix  $s_{\min}$  and a convergence criterion  $\epsilon$  for the obtained frequencies.<sup>38</sup> They were chosen as  $s_{\min} = 10^{-8}$  and  $\epsilon = 10^{-6}, \dots, 10^{-3}$ .

### 5. Wigner function

To gain insight into the state created by the pulse, a phase space picture is employed. A Wigner function<sup>40,41</sup> of the primary system density operator, either on the ground or excited electronic surface, is used:

$$W_S(P, Q) = \frac{1}{2\pi} \int \hat{\rho}_S(Q - y/2, Q + y/2) e^{iPy} dy. \quad (22)$$

Unlike a classical probability density, the Wigner distribution can have negative values. The existence of these negative values indicates regions in phase space which are dominated by pure quantum phenomena.

## III. THE DIFFERENT DISSIPATION PROCESSES AS DESCRIBED BY THE SURROGATE HAMILTONIAN

The bath has a strong influence on all aspects of the dynamics. Traditionally this influence is classified as energy relaxation ( $T_1$ ) and energy dephasing ( $T_2$ ). These processes influence both the nuclear degrees of freedom and the electronic degrees of freedom.<sup>8</sup> The following Hamiltonian describes these possibilities:

$$\hat{H}_{SB} = \hat{H}_{SB}^{nr} + \hat{H}_{SB}^{er} + \hat{H}_{SB}^{nd} + \hat{H}_{SB}^{ed}, \quad (23)$$

where  $nr$  means nuclear relaxation,  $er$  electronic relaxation,  $nd$  nuclear dephasing and  $ed$  electronic dephasing. Details of these system-bath coupling operators with illustrative examples are presented below.

### A. Energy relaxation processes

Energy relaxation is an exchange of energy between system and bath which will lead eventually to thermal equilibrium. The process can be imagined as taking energy out of the primary system and simultaneously creating an excitation in a bath mode. The inverse process of destroying an excitation in a bath mode and transferring this energy to the system is also possible.

The operator describing the exchange of energy of the bath modes with the nuclear degrees of freedom is a generalization to two electronic surfaces of the interaction term used in previous studies:<sup>12</sup>

$$\hat{H}_{SB}^{nr} = \begin{pmatrix} f_g(\hat{Q}) & 0 \\ 0 & f_e(\hat{Q}) \end{pmatrix} \otimes \sum_i d_i^{nr} (\hat{\sigma}_i^\dagger + \hat{\sigma}_i), \quad (24)$$

where  $f_{e/g}(\hat{Q})$  are functions of the system displacement operator. This means that the system-bath coupling can be different for the ground or excited state potential. The constants  $d_i^{nr}$  are determined from the spectral density:

$$d_i^{nr} = \sqrt{J(\epsilon_i)/\rho(\epsilon_i)}, \quad (25)$$

where  $\rho(\epsilon_i)$  is the density of states of the bath. Assuming an Ohmic form, the spectral density becomes

$$J(\epsilon) = \eta \epsilon e^{-\epsilon/\epsilon_c}. \quad (26)$$

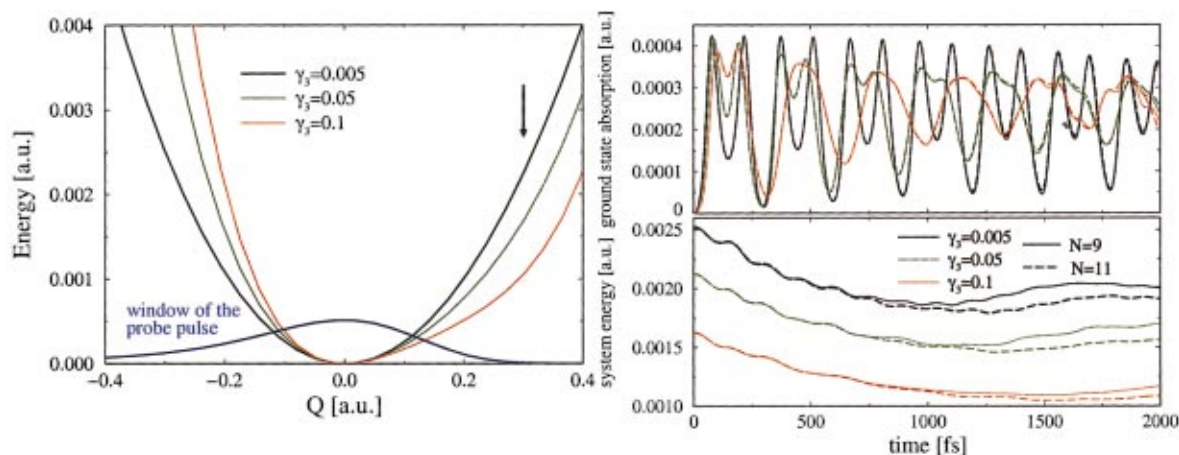


FIG. 2. (Color) Potentials for the anharmonic oscillator with increasing third order term  $\gamma_3$  given in the legend. The arrow indicates the position of the initial state. The window operator which was used to calculate the absorption is also plotted. The average energy as a function of time for increasing anharmonicity (bottom) and the ground state absorption for increasing anharmonicity (top) are shown on the right.  $N$  is the number of bath modes, the system-bath coupling is  $\eta=2$  and the cutoff frequency is  $\varepsilon = \omega_g$ .

The interaction with the bath can also lead to electronic quenching described by the interaction

$$\hat{\mathbf{H}}_{SB}^{er} = \frac{1}{2} \begin{pmatrix} 0 & 1 \\ 1 & 0 \end{pmatrix} \otimes \sum_i d_i^{er} (\hat{\sigma}_i^\dagger + \hat{\sigma}_i). \quad (27)$$

A similar relation as Eq. (25) holds for the  $d_i^{er}$ , but the spectral density will be different.

The vibrational relaxation in the surrogate Hamiltonian model has been tested previously for the standard model of a harmonic oscillator interacting with a bath.<sup>12</sup> Nevertheless the grid representation of the primary system allows for the treatment of a general anharmonic potential. The vibrational relaxation study is extended therefore to the case of an anharmonic oscillator in a bath (Fig. 2). The anharmonic part of the potential is given by third and fourth order terms in  $\hat{Q}$ :

$$V_{\text{anh}} = \gamma_3 \hat{Q}^3 + \gamma_4 \hat{Q}^4, \quad (28)$$

where  $\gamma_3$  was used as free parameter and  $\gamma_4$  was chosen to balance the third order term,  $\gamma_4 = -\gamma_3/Q_{cr}$  with  $Q_{cr}$  from Eq. (34). The initial state was a displaced correlated ground state of the system and bath, which was displaced by  $Q_0 = 0.3$  a.u. as indicated in Fig. 2. The qualitative shapes of the energy relaxation curves for different anharmonicities shown in Fig. 2 are quite similar. Examining the left part of Fig. 2, it becomes clear that with increasing anharmonicity the average initial energy decreases. With 11 bath modes, the method converges to a time scale of  $\sim 1000$  fs. The artificial recurrence of the energy for the harmonic case after  $\sim 1000$  fs should be noticed (Fig. 2). For anharmonic cases, the recurrence is less significant due to a spread of the system energy to more bath modes. Larger differences due to the anharmonicity are observed in the absorption of a probe pulse (top right of Fig. 2). Due to the position of the window function the second harmonic component is enhanced which is the result of the double passage of the wave packet for each vibrational period. The decay of spectral modulations is faster when the anharmonicity increases, in particular the double peak reflecting the second harmonic component is

lost much faster. These observations are similar to the ones seen in a vibrational relaxation model based on solving the semi-group Liouville von Neumann equation.<sup>16</sup> This phenomenon is the result of the initially compact wave function getting out of phase when the energy level spacing is not constant because the dissipative forces originating from the bath exclude coherent revival of the wave packet.<sup>42</sup>

## B. Introduction of dephasing into the surrogate Hamiltonian

Dephasing is a process caused by an almost elastic interaction between system and bath which alters the accumulated phase of the system. A qualitative picture is based on an almost elastic exchange of energy between two bath modes. This is described by creating an excitation in one mode at the expense of an excitation in another mode, and vice versa. This process modulates the Hamiltonian of the primary system. From this description it is clear that for dephasing to take place the bath has to be initially excited. Therefore, when the temperature is decreased, dephasing processes are frozen. For nuclear dephasing, the bath modulates the vibrational Hamiltonian:

$$\hat{\mathbf{H}}_{SB}^{nd} = \begin{pmatrix} \hat{\mathbf{H}}_g & 0 \\ 0 & \hat{\mathbf{H}}_e \end{pmatrix} \otimes \sum_{ij} c_{ij}^{nd} (\hat{\sigma}_i^\dagger \hat{\sigma}_j + \hat{\sigma}_j^\dagger \hat{\sigma}_i). \quad (29)$$

The coefficients  $c_{ij}$  are biased to represent almost elastic encounters,

$$c_{ij} = \bar{c} e^{-(\varepsilon_i - \varepsilon_j)^2 / 2\sigma_\varepsilon^2}, \quad (30)$$

with  $\bar{c}$  a global dephasing parameter, and  $\sigma_\varepsilon$  determines the inelastic bias. We found the dephasing rate to be proportional to the square of the band width of  $c_{ij}$ .

Pure vibrational dephasing leads to a spreading of the wave packet in phase space, shown in Fig. 3 where the ground state of a harmonic potential was displaced and evolved in time. The sign of each individual term  $c_{ij}^{nd}$  in Eq. (29) determines if its contribution advances the phase (nega-

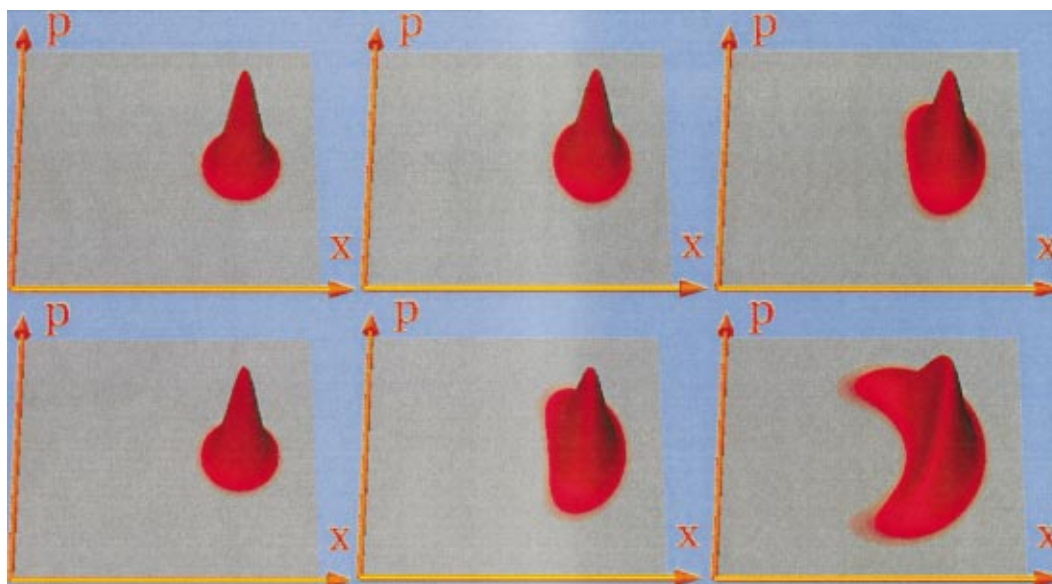


FIG. 3. (Color) The Wigner function of an initially displaced Gaussian state in a harmonic potential. The state is plotted after 0, 2 and 4 periods for the nuclear dephasing parameter  $\bar{c}=0.2$  (top) and for  $\bar{c}=0.5$  (bottom). Nuclear dephasing leads to a spreading of the wave packet which occurs faster for stronger dephasing.

tive  $c_{ij}^{nd}$ ) or delays it (positive  $c_{ij}^{nd}$ ). A random choice of the sign of  $c_{ij}^{nd}$  will cause a phase diffusion in both directions without affecting the average phase propagation determined by  $\hat{H}_S$ .

Higher harmonic motion was generated by placing two, three and four Gaussian wave packets symmetrically on a specified ellipse in phase space. The transient absorption at the turning point of this initial state was recorded and fitted with the use of the filter diagonalization method. The frequencies with the highest amplitudes were the second, third and fourth harmonics. Analysis of the decay rates corresponding to these frequencies shows a 1:2 ratio between the first and second harmonics, 1:3 between the first and third harmonics and 1:4 between the first and fourth harmonics. These ratios deviate from the 1:4, 1:9 and 1:16 ratios expected in a Gaussian dephasing model, and indicate that the dephasing mechanism is Poisson-like.<sup>43</sup>

For electronic dephasing, the bath modulates the electronic excitation:

$$\hat{H}_{SB}^{ed} = \Delta_V(\hat{Q}) \frac{1}{2} \begin{pmatrix} -1 & 0 \\ 0 & 1 \end{pmatrix} \otimes \sum_{ij} c_{ij}^{ed} (\hat{\sigma}_i^\dagger \hat{\sigma}_j + \hat{\sigma}_j^\dagger \hat{\sigma}_i). \quad (31)$$

$\Delta_V(\hat{Q})$  is the difference potential describing the dependence of the modulation on the nuclear displacement.

The effect of pure electronic dephasing is shown in Figs. 4 and 5, where a two-level system is excited by a  $\pi$ -pulse on resonance. The initial state was chosen such that the system is in its ground state and the bath states are partially populated. For the zero dephasing case, the  $\pi$ -pulse leads to a complete population inversion. Once dephasing is included, the amount of population transfer decreases, eventually reaching 50% conversion which corresponds to a random electronic phase. For stronger dephasing, more modes are required to obtain converged results. The total energy absorbed from the pulse has been calculated by use of Eq. (13).

By varying the carrier frequency of the pulse, a spectrum of power versus frequency has been obtained. The minimum width of the spectrum is determined by the Fourier transform of the pulse. Once dephasing is introduced the frequency of the absorption peak is shifted corresponding to the initial value of the system-bath interaction energy  $\langle \hat{H}_{SB}^{ed} \rangle$ . An additional dynamical shift is also observed which is linear in  $c_{ed}$  for small values and reaches saturation at higher values. The dephasing also adds an additional width to the peak which scales quadratically with the dephasing parameter (Fig. 5). The quadratic scaling of the width with the dephasing constant  $c^{ed}$  as well as with the band width indicates that the surrogate Hamiltonian dephasing process is second order in the system-bath coupling. This is consistent with derivations

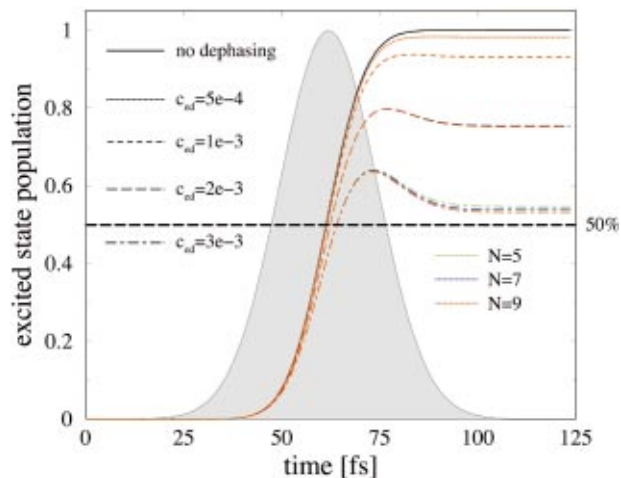


FIG. 4. (Color) Electronic dephasing: Decrease of population excited by a  $\pi$ -pulse for increasing dephasing strength  $c_{ed}$ ,  $N$  is the number of bath modes. The pulse envelope (not to scale) is shown in the background.

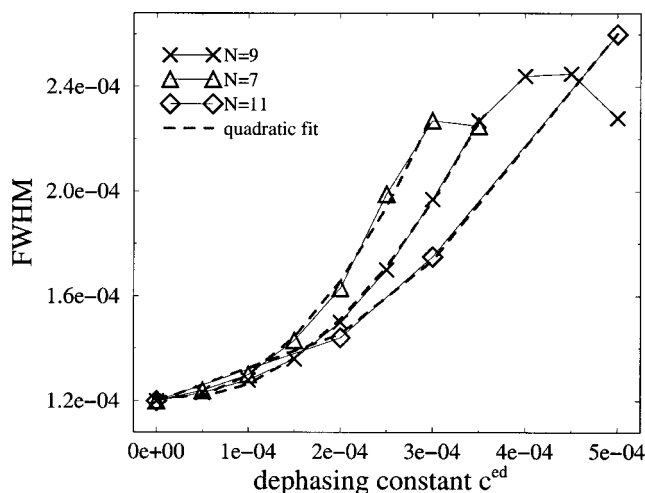


FIG. 5. The FWHM of the pulse spectrum as a function of dephasing constant  $c^{ed}$  for increasing number of bath modes. The deviation from a quadratic fit indicates the breakdown of convergence.

of Redfield theory based on time-dependent perturbation theory in the system-bath coupling.<sup>44</sup>

The above examples demonstrate the ability of the surrogate Hamiltonian method to model the four isolated dissipative phenomena and to establish the requirements for convergence.

#### IV. RESULTS

Once the individual dissipative phenomena have been modeled, the full photoreaction cycle can be described. The electronic potential energy levels are chosen to be the traditional displaced harmonic oscillators:

$$V_g(\hat{Q}) = \frac{1}{2} M \omega_g^2 \hat{Q}^2, \quad (32)$$

$$V_e(\hat{Q}) = \frac{1}{2} M \omega_e^2 (\hat{Q} - Q_0)^2 + \Delta, \quad (33)$$

where  $\omega_{g/e}$  are the vibrational frequencies of the ground and excited surfaces,  $Q_0$  is the shift in equilibrium position and  $\Delta$  is the energy shift between the minima. Other nonharmonic potentials have been modeled by adding a cubic and quartic term to the potentials (cf. Sec. III A). The system parameters were chosen as  $\omega_g = 5.0e-4$ ,  $\omega_e = 0.7\omega_g$ ,  $Q_0 = 0.2$  and  $\Delta = 0.004$  (all in atomic units). The diabatic coupling potential is described as

$$V_d(\hat{Q}) = J_d e^{-\frac{(\hat{Q} - Q_{cr})^2}{2\sigma_d^2}}, \quad (34)$$

where  $Q_{cr}$  is the position of the maximum coupling point,  $\sigma_d$  is the variance of the coupling function and  $J_d$  its amplitude. By varying the parameters of the diabatic coupling its influence can change from a localized effect at  $Q_{cr}$  to a constant function independent of  $Q_{cr}$ .

The pump pulse envelope was modeled as a Gaussian:

$$E(t) = E_0 e^{-(t-t_{max})^2/2\sigma_L^2} e^{-i\omega_L t} \quad (35)$$

with the intensity  $E_0$  adjusted such that  $\approx 10\%$  of the ground state population was transferred to the excited state which is typical in the experiments.<sup>30</sup> The carrier frequency  $\omega_L$  was chosen to match the difference between the ground and ex-

cited electronic potentials at the minimum of the ground state. The width (FWHM) of the pulse which is connected to  $\sigma_L$  was chosen as 20 fs which is approximately  $\frac{1}{10}$  of the ground state vibrational period and  $\frac{1}{15}$  of the excited state vibrational period, typical for charge transfer experiments.<sup>11</sup>  $t_{max}$  was fixed by starting the propagation at  $t_0 = t_{max} - 3\sigma_L$ . The probe pulse profile was identical to the pump pulse profile but with 10% of the pump intensity.

#### A. Equilibration of the initial state

Once the system-bath Hamiltonian is set, the correlated ground state can be determined by propagating an initial guess wave function in imaginary time  $\tau$ :

$$\Psi(\hat{Q}; \tau) = e^{-\hat{H}\tau} \Psi(\hat{Q}; 0). \quad (36)$$

As  $\tau$  is increased this state will converge exponentially to the ground state. Low lying excited states are obtained by filtering out the previously found lower states and repeating the propagation process.<sup>45</sup> For temperatures which are low relative to the electronic energy difference  $k_B T \ll \Delta$ , the initial state can be determined using only the ground surface Hamiltonian.

The energy stored in the system-bath coupling,  $\langle \hat{H}_{SB} \rangle$ , was computed. Its value depends on the coupling parameter. In our simulations we could get converged results for relatively large coupling with  $\langle \hat{H}_{SB} \rangle$  reaching 30% of the total energy. In spite of this, the effect of initial correlations on the dynamics was found to be small even for the strong coupling case. The autocorrelation function and the transient emission were compared for a correlated and an uncorrelated initial state. In the uncorrelated case, the initial state is the ground state of  $\hat{H}_g$ , while in the correlated case it is the ground state of  $\hat{H}_g + \hat{H}_{SB}^{nr} + \hat{H}_B$ . The comparison was made with a set of different coupling functions  $f_{g/e}(\hat{Q})$  in Eq. (24) and the observed effect was small for linear as well as nonlinear coupling. In both cases the system-bath coupling term caused a significant shift of the modulation frequency. The influence of initial correlation has also been addressed in the context of the weak coupling approximation<sup>14</sup> where it appears as an additional inhomogeneous term.

#### B. CW absorption spectra

The CW absorption spectrum reflects part of the photoreaction dynamics. The time-dependent approach is used to calculate the CW absorption cross section employing Eqs. (17) and (19). At  $t=0$  the ground state of the electronic ground state potential is promoted onto the electronic excited state and the diabatic coupling as well as the coupling to the bath are switched on. The frequency of the ground state potential was chosen to be  $\omega_g = 10^{-3}$  a.u., i.e., about  $220 \text{ cm}^{-1}$ , and the frequency of the excited state potential  $\omega_e = 0.7\omega_g$ . Figure 6 shows the autocorrelation function of Eq. (17) (on the left) and the absorption cross section Eq. (19) (on the right) for constant diabatic coupling (top) and for localized diabatic coupling (bottom). Since the surrogate Hamiltonian is converged only for a finite time the autocorrelation function cannot be Fourier transformed directly. Instead the frequencies

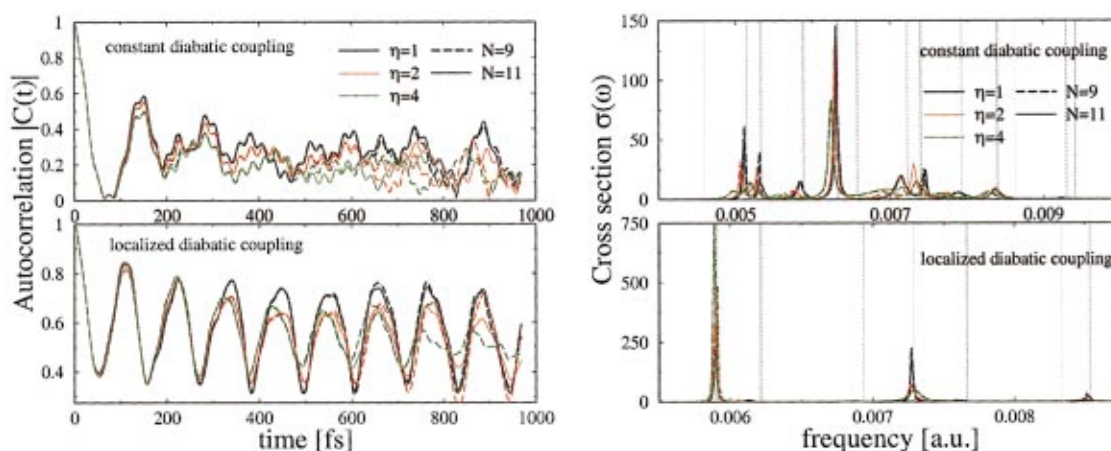


FIG. 6. (Color) The autocorrelation function (on the left, the absolute value is plotted) and the corresponding absorption cross section (on the right) for constant diabatic coupling,  $J_d = \omega_g$ , (top) and localized diabatic coupling,  $J_d = 5\omega_g$ ,  $\sigma_d = 0.1$  (bottom), and for increasing system-bath coupling  $\eta$ . The eigenfrequencies of the system Hamiltonian are indicated by the thin gray lines.

and decay rates contained in the signal were extracted from a finite observation window by filter diagonalization. The CW absorption spectrum was then reconstructed by a sum of Lorentzians. The data window in time was confined by the convergence time of the surrogate Hamiltonian, indicated by comparing the  $N=9$  to the  $N=11$  modes. The actual data window had to be chosen carefully since it is used for extrapolation to longer times. In Fig. 6 the data between 50 and 530 fs were used.

In addition to the spectrum, the eigenfrequencies of the system Hamiltonian  $\hat{H}_S$ , including the diabatic coupling, are indicated as thin lines in Fig. 6. The nonstationary initial state can be expanded into eigenstates of the system as can be seen in Fig. 6. In the case of the constant diabatic coupling all eigenstates within a certain energy range are excited while for the localized diabatic coupling only a few eigenstates contribute. In case of localized coupling, see Fig. 6 bottom right, the eigenstates corresponding to the three peaks with highest intensity carry 80% of their weight on the excited state while the eigenstates in between carry less intensity on the electronically excited state. For constant diabatic coupling more peaks are excited, see Fig. 6 top right. In this case it is the eigenstates with peaks close to the classical turning point which contribute most. The influence of the

bath is twofold: It leads to a finite width of the peaks which increases with increasing system-bath coupling  $\eta$ . Furthermore, the bath shifts the spectrum first towards lower frequencies but then due to mixing the frequencies can increase (cf. Sec. IV D).

### C. Excitation by the pump pulse

The initial state on the ground electronic surface is also the starting point for launching the pump-probe simulation. This state is propagated with the time-dependent Hamiltonian leading to population transfer to the excited state. Figure 7 shows the phase space density of the excited state wave function at different times during the pump pulse. Due to the slope of the excited state potential the population transfer is not symmetric (Fig. 7, left and middle). Towards the end of the pump pulse duration, the wave packet starts to move away from the Franck–Condon point and develops a coordinate-momentum correlation. In almost all previous studies of the charge transfer problem, the initial state was chosen to be an uncorrelated Gaussian wave packet positioned at the FC point on the excited electronic state and a global diabatic coupling was switched on at  $t=0$ . When the excitation process induced by the pump pulse is considered

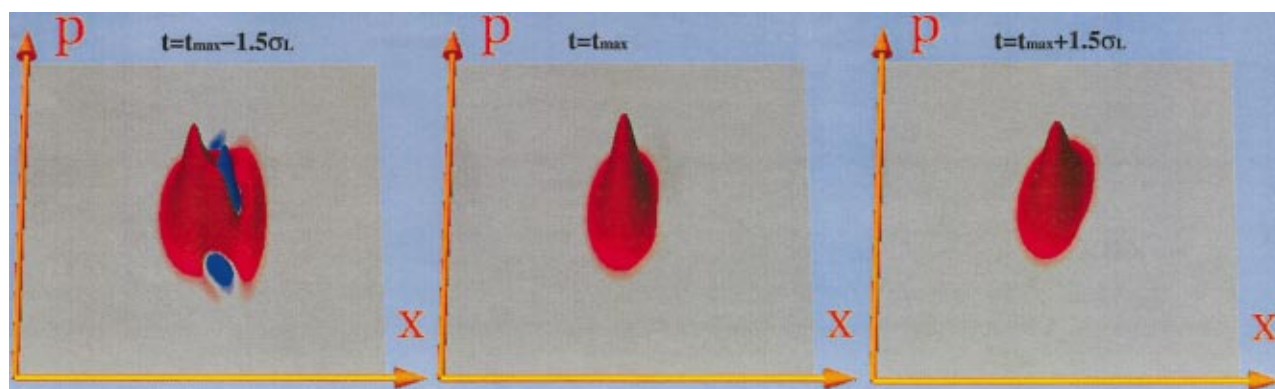


FIG. 7. (Color) Normalized Wigner function for the excited state wave function during the pump pulse at  $t = t_{\max} - 1.5\sigma_L$ ,  $t = t_{\max}$ , and  $t = t_{\max} + 1.5\sigma_L$  (from left to right) with  $\omega_e = 0.7\omega_g$ ,  $\eta = 1.0$ ,  $J_d = 5\omega_g$ ,  $\sigma_d = 0.1$ , and  $N_{\text{modes}} = 11$ .

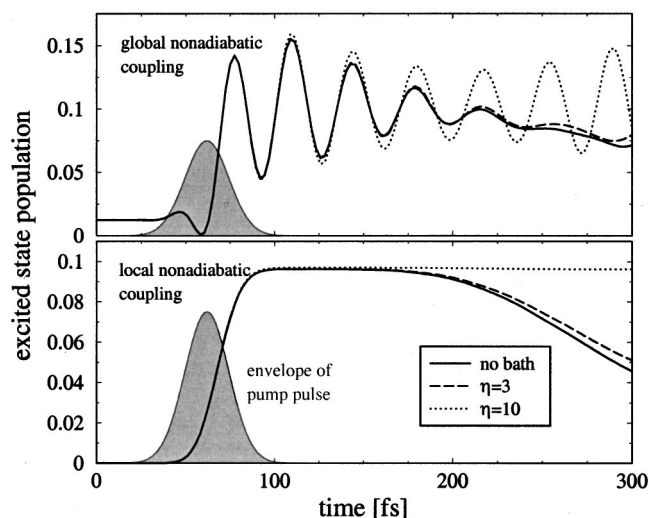


FIG. 8. The population on the excited state for global and for local diabatic coupling ( $J_d=1.0\omega_g$ ,  $\sigma_d=0.1$ ), with and without vibrational relaxation ( $\eta$ ). The initial state, which is the ground state of the total system and bath, is partially excited to the electronically excited state due to the pump pulse (indicated).

explicitly, this choice of the diabatic coupling leads to unphysical spurious results. This is shown in the upper panel of Fig. 8. Due to the global diabatic coupling, the excited state is already populated before the excitation. Therefore the pump pulse results in both stimulated absorption and emission. Furthermore, this choice of diabatic coupling immediately induces population transfer between the electronic states (see the oscillations in Fig. 8, upper panel). A fix to this unphysical problem is obtained by a localized diabatic coupling operator (Fig. 8, lower panel). Diabatic coupling functions obtained from *ab initio* calculations turn out to be localized.<sup>46,47</sup> For this case the electronic excited state is not

populated initially, and population transfer starts only after the pump pulse has been applied and the wave packet has traveled to the crossing region of the potentials. For localized diabatic coupling and strong vibrational relaxation, a new phenomenon can be observed: trapping on the excited state. In this case, the wave packet relaxes so fast that it can not reach the crossing region of the potentials anymore. This observation is part of the turnover phenomenon (cf. Sec. IV E).

#### D. Absorption of the probe pulse and “recovery of the bleach”

The absorption of the probe pulse reflects the ground state dynamics. Figure 9 displays the Wigner function of the ground state wave packet after the excitation and Fig. 10 shows several dynamical expectation values. The time steps at which the Wigner function was plotted are indicated by arrows in the middle panel of Fig. 10. Since the pump pulse excites  $\sim 10\%$  of the ground state population to the excited state, the ground state wave packet is only weakly perturbed by the excitation process. However, after the excited state wave packet has reached the crossing point, population is nonadiabatically transferred back to the ground state. Due to the locality of the diabatic coupling, this population transfer occurs in spurts. On the excited state surface the Wigner function splits when it hits the crossing point. In Fig. 10 one observes the loss of ground state population due to the pump pulse and then the recovery of the population due to nonadiabatic transfer (middle panel). The newly created population on the ground electronic surface is vibrationally excited (top panel). The appearance of this population in the observation window of the probe is delayed by the time scale of vibrational relaxation (cf. Fig. 11 left, bottom panel). This phenomenon has been termed the “recovery of the bleach.”

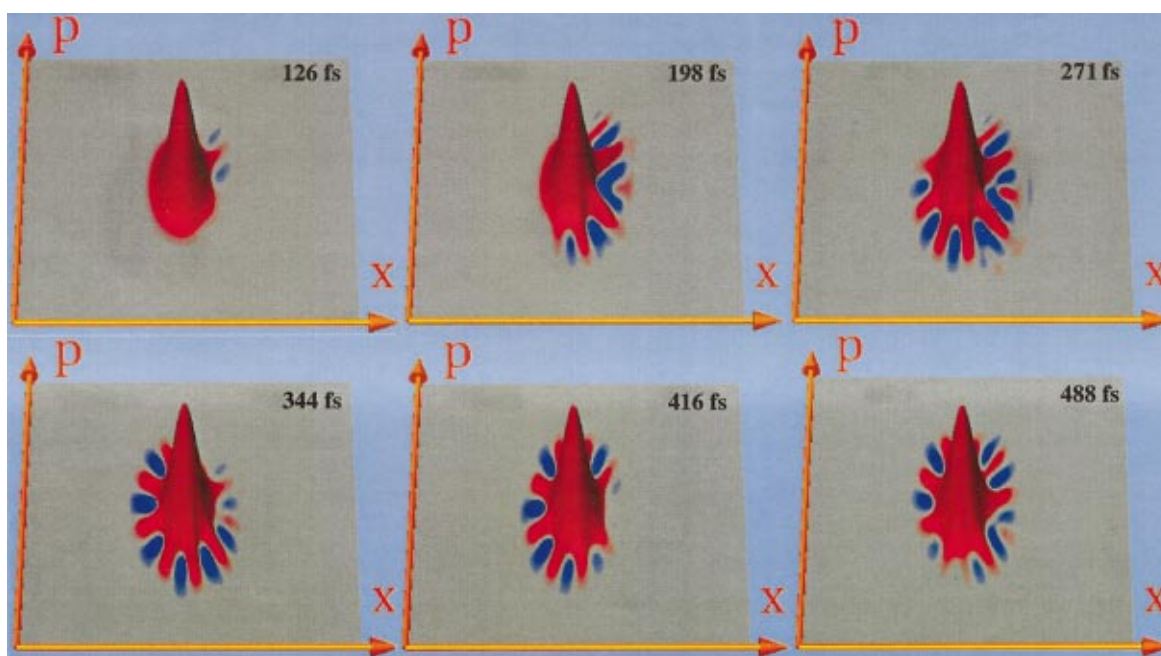


FIG. 9. (Color) The Wigner function of the ground state wave function at subsequent times (126, 198, 271, 344, 416, and 488 fs from top left to bottom right). The system-bath coupling is  $\eta=1\omega_g$  and the local diabatic coupling is  $J_d=5\omega_g$ , with width  $\sigma_d=0.1$ .

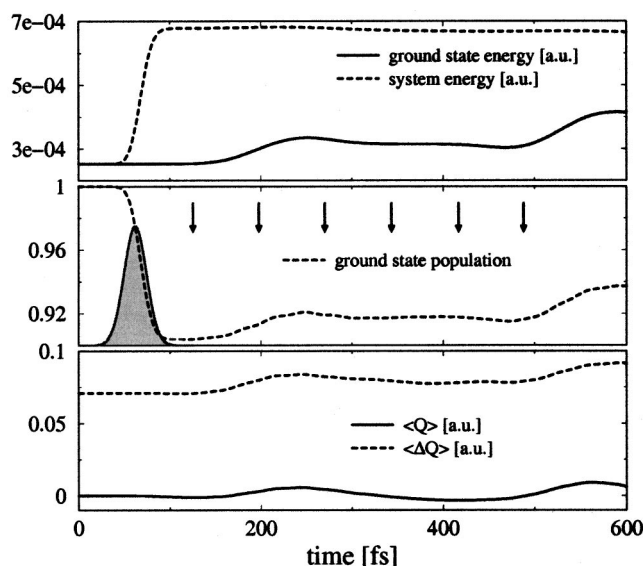


FIG. 10. Expectation values of  $\hat{H}_g$  and  $\hat{H}_s$  (upper panel), the ground state population (middle panel), and the expectation value of  $\hat{Q}$  and  $\Delta\hat{Q} = \sqrt{\langle\hat{Q}^2\rangle - \langle\hat{Q}\rangle^2}$  on the ground state (lower panel) vs time. The envelope of the pump pulse and the times at which the Wigner function is plotted in Fig. 9 are indicated.

Finally, the transient absorption and emission signals and their spectra are plotted in Fig. 11. Higher harmonics corresponding to the non-Gaussian features in the Wigner function (Fig. 9) can be observed (see insets in Fig. 11). These features could not be seen in the coordinate expectation value,  $\langle\hat{Q}\rangle$ , or the coordinate standard deviation,  $\langle\Delta\hat{Q}\rangle$  (Fig. 10, bottom panel). Figure 11 shows furthermore the influence of electronic dephasing on the transient emission and absorption signals. Nuclear dephasing with reasonable parameters did not influence the dynamics.

The shape of the transient emission/absorption is caused by both electronic oscillations and nuclear vibrations. Therefore the observed frequencies do not correspond to the vibra-

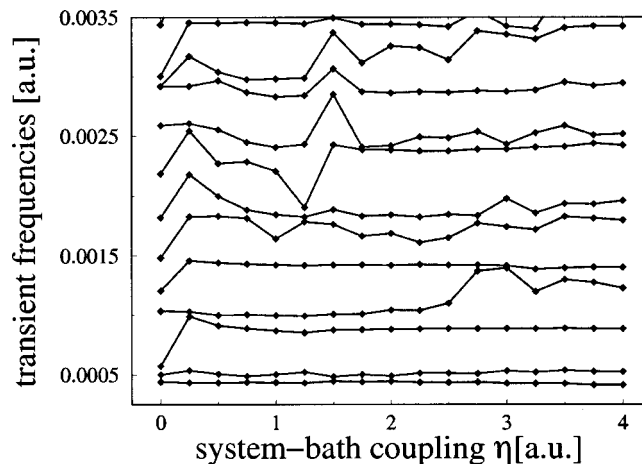


FIG. 12. Frequencies in the transient ground state absorption obtained by filter diagonalization vs the system-bath coupling parameter. No electronic dephasing is included. The remaining parameters are the same as in the previous figure.

tional frequencies of the diabatic potentials or to the eigenvalues of the system Hamiltonian  $H_S$  (in contrast to the absorption cross section, cf. Sec. IV B). The observed frequencies are rather a result of a subtle interplay between system and bath. To illustrate this, the system-bath coupling parameter was varied and the frequencies of the ground state absorption, obtained by filter diagonalization, are plotted versus the system-bath coupling in Fig. 12. A pattern of avoided crossings as a function of the system-bath coupling parameter  $\eta$  is clearly visible.

The amplitude of the electronic oscillations is decreased by electronic dephasing, and this leads to a decrease in amplitude of the oscillations in the transient emission/absorption (Fig. 11, left). Filter diagonalization was applied to obtain spectra, and a data window between 250 and 1410 fs was chosen. Dephasing causes a widening of the peaks in the spectra (Fig. 11, right).

The “recovery of the bleach” or the recovery of the

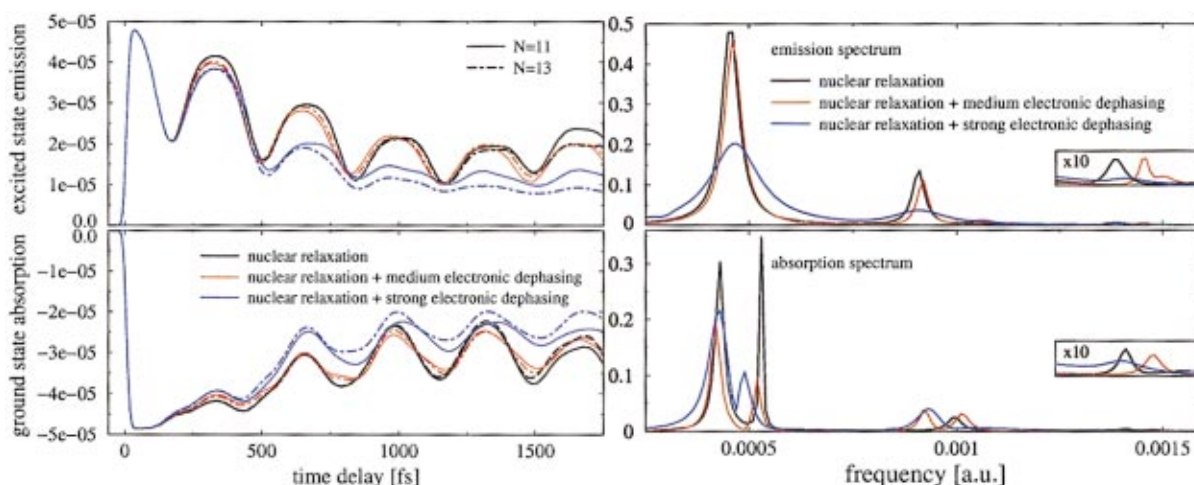


FIG. 11. (Color) Stimulated transient emission (left, upper panel) and transient absorption (left, lower panel) and their spectra (right) for nuclear relaxation and for nuclear relaxation with electronic dephasing. The relaxation parameter is  $\eta=1$  with cutoff frequency  $\varepsilon_c=2\varepsilon_g$ ; the dephasing parameter is  $\bar{c}=0.005$  for medium dephasing and  $\bar{c}=0.01$  for strong dephasing. The pump and probe frequencies are chosen to correspond to the bottom of the ground electronic potential.

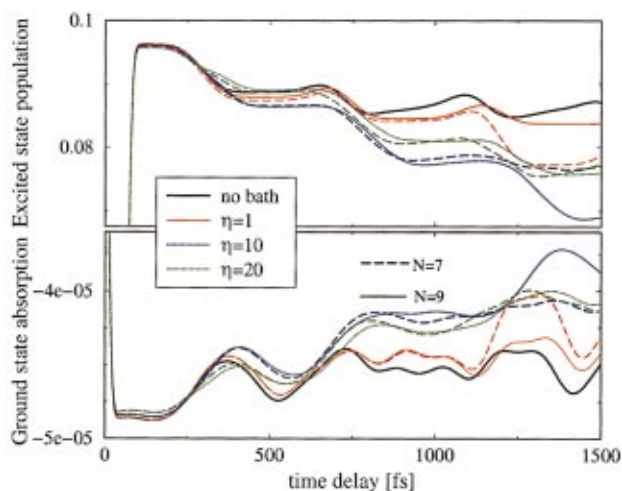


FIG. 13. (Color) Turnover: The population of the excited state (upper panel) and the ground state transient absorption (lower panel) for different  $\eta$  with the parameters of the diabatic coupling  $J_d = \omega_g$  and  $\sigma_d = 0.1$ .

ground state absorption is observed in the bottom left panel of Fig. 11. This recovery is due to filling of the observation window, Eq. (15), caused by the nonadiabatic transfer from the excited state and by cooling of the vibrational excitation on the ground electronic potential (see Fig. 1).

The probe pulse can be positioned in resonance to the inner and outer turning points of the ground state potential. One would expect a half-period time delay between the peaks in the two signals.<sup>11</sup> We found that the electronic oscillations due to the nonadiabatic population transfer completely destroy this half-period time delay pattern.

The time scale for the recovery which corresponds to the decay rate of zero frequency is  $\sim 1.5$  ps. To estimate the influence of dephasing the highest peak intensities were compared. For data windows between 770 and 1430 fs, a linear dependence of the intensity versus the dephasing parameter was obtained and the slope varied between  $-0.9e-4$  and  $-1.5e-4$ .

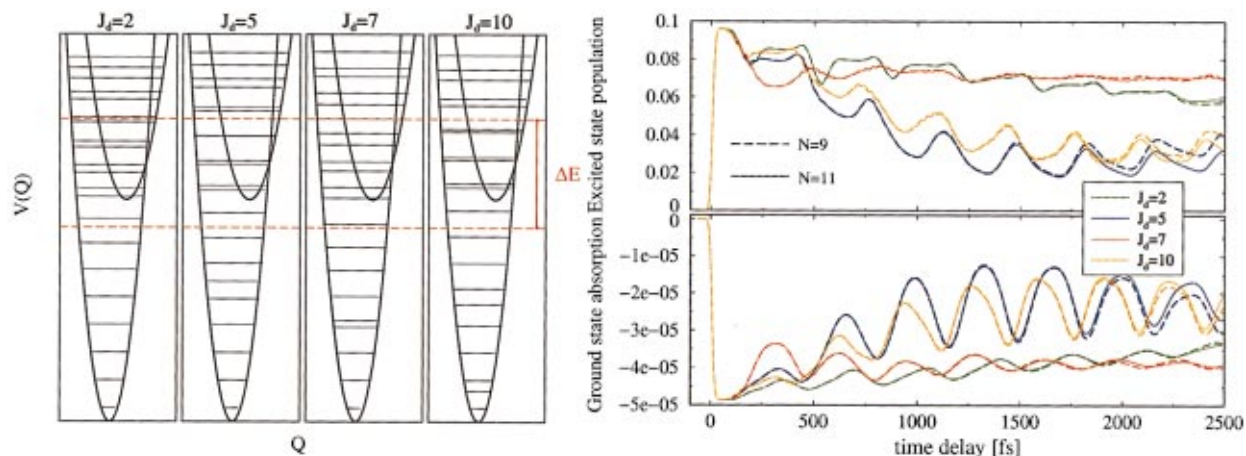


FIG. 14. (Color) Turnover: Resonance phenomenon due to variation of  $J_d$ . The diabatic potentials with the energy levels of  $H_S$  are shown on the left, also plotted is the band width  $\Delta E$  due to the pulse. For  $J_d = 5$  and  $J_d = 10$  there are quasi-degeneracies within the energy window given by  $\Delta E$ . This leads to an enhanced population transfer (right, upper panel) which can be detected in the ground state absorption (right, lower panel).

## E. Turnover behavior

This study points to the complexity of the nonadiabatic charge transfer event. The phenomenon is sensitive to all dynamical parameters. Previously, based on a semi-group model of dissipation, Ashkenazi *et al.*<sup>8</sup> have observed a turnover of the charge transfer rate as a function of almost any external variable, i.e., the rate first increased and then decreased as a function of the nuclear relaxation or the nuclear dephasing rate, the electronic dephasing rate, as well as of the diabatic coupling parameter  $J$ . Figure 13 demonstrates the turnover phenomenon as a function of the nuclear relaxation rate. The excited state population is first created by the pump and then lost through the diabatic coupling to the ground state. The rate of loss increases with  $\eta$  but then the turnover takes place and the population becomes trapped on the lowest part of the well of the excited state. From this position the nonadiabatic transfer can occur only by tunneling, which is slow relative to the other processes. The transient absorption of the probe pulse from the ground state reflects the increase in population which is known experimentally as the “recovery of the bleach.”<sup>11</sup> The slow recovery of the bleach for high  $\eta$  means that the turnover phenomenon can be observed by pump-probe ultrafast spectroscopy.

A more complex turnover phenomenon is observed with respect to the diabatic coupling constant  $J_d$ . In addition to a general turnover trend, oscillations in the rate as a function of  $J_d$  are observed (cf. Fig. 14). These oscillations can be attributed to accidental degeneracies between the electronic ground and excited state (cf. Fig. 14 left). These degeneracies are not observed in the global diabatic coupling case.

## V. CONCLUSIONS

The present study is the first construction of a comprehensive model for ultrafast pump-probe spectroscopy of the charge transfer cycle. The use of the surrogate Hamiltonian has the advantage of a consistent treatment of initial correlation, non-Markovian dynamics and explicit description of the pulse field. This exploration has identified severe flaws in

previous descriptions.<sup>8,48,49</sup> The main flaw is in the Franck–Condon choice of a vertical transition of the ground state as the initial state for the nonadiabatic process. This choice ignores the initial system-bath correlation and the dynamical aspects of the pump pulse. It was found that the initial system-bath correlation has only a small influence on the short-time observables investigated here. However, an effect of initial correlations on nonexponential long-time dynamics has been reported within a path integral approach on a single surface.<sup>50</sup> The system-bath coupling causes a large dynamical influence in combination with the nonadiabatic character of the excited vibrational eigenstates, it induces mixing of the states resulting in a complicated pattern of frequency shifts. The phase shift between different locations of the probe pulse transition does not correspond to simple ground surface coherent motion. Moreover, the pulse induced population transfer to the excited surface is strongly influenced by the diabatic coupling term as well as by the electronic dephasing term. The analysis shows that only the localized version of the diabatic coupling term has physical meaning.

The construction of the charge transfer model has required new methodological developments in the surrogate Hamiltonian method. The first step taken was to extend the system's description by including both nuclear and electronic degrees of freedom. The next important step was the introduction of both nuclear and electronic dephasing terms. For a chromophore in a bath, electronic quenching is not effective since there are no dipoles in the solvent which are in resonance with the electronic transition dipole. This situation could change for chromophores on metal or semiconductor surfaces where electronic quenching can be significant due to bath modes in the appropriate frequency range.

The utility of the method was significantly enhanced by the incorporation of the filter diagonalization method. Since in practice the surrogate Hamiltonian method describes short time dynamics it is necessary to extrapolate to longer times to obtain relaxation data and frequency domain spectra. The filter diagonalization method fits the data in a time window to a sum of complex exponentials. This comes as a surprise since the dynamics is generated by a Hamiltonian and therefore it is unitary and it should only show oscillatory behavior causing the filter diagonalization method to extract pure frequencies. The fact that we could obtain finite decay rates is a result of the finite precision and the finite frequency window of the filter diagonalization. The recurrences of the unitary time evolution do not show up numerically within the convergence time window. For infinite precision and an infinite frequency range the filter diagonalization method would “detect” the recurrences even if a finite data window within the convergence time is used. Therefore the combination of the surrogate Hamiltonian with the filter diagonalization method is successful due to the finite-precision numerical representation of the problem.

Modeling quantum dissipative phenomenon is an extremely difficult task. The surrogate Hamiltonian method is one of a few alternative approaches. The only other method which has addressed the problem of external fields and initial correlation is the weak coupling non-Markovian approach of Meier and Tannor<sup>19</sup> and Geva, Rosenman, and Tannor.<sup>14</sup>

Their method is based on a reduced description which describes explicitly the dynamics of the system in Liouville space. Work on comparing the two methods is in progress. Preliminary results show the surrogate Hamiltonian to have advantages at low bath temperatures while at high temperatures the Liouville approach takes over. The reason for this is that for higher temperatures, the calculation has to be repeated with a large ensemble of excited initial states. Other reduced descriptions such as the empirical semi-group approach<sup>51</sup> cannot cope with the full scope of pump-probe charge transfer dynamics. Path integral methods<sup>22</sup> are not able, at present, to fully model the time-dependent dynamics of the charge transfer process.

The present study does confirm the general turnover phenomenon in the charge transfer reaction<sup>8</sup> which was first identified in a qualitative semi-group study. The physical source of the turnover is the noncommutability of the system Hamiltonian with the system-bath coupling terms. The present modeling of the pump-probe experiment shows that the transient absorption can be used to indicate the turnover phenomenon. The turnover phenomenon also imposes restrictions on the maximum rate which can be observed in the recovery of the bleach. With the current set of parameters this time scale is approximately 1.5 ps which is a factor of 2 slower than the experimental findings.

One of the striking features of the charge transfer cycle is its complexity. The nonadiabatic dynamics is found to be sensitive to all internal system parameters as well as system-bath coupling elements. Nevertheless, the present model is still over-simplified. The main discrepancy is the result of the single nuclear degree of freedom. It is well documented that nonadiabatic transfer events are extremely sensitive to the nuclear topology.<sup>52</sup> An additional nuclear degree of freedom allows the existence of conical intersections which open a new fast route or funnel from the excited to the ground state.<sup>48</sup> This could be the reason for the discrepancy between the current 1-D calculations and the experimental findings. In principle the description of the primary system could be extended to include additional degrees of freedom. This addition would tax heavily the required computational resources. However, adding a single high frequency vibrational mode becomes feasible by just including the two lowest levels as an additional spin. An additional electronic degree of freedom would be described in a similar fashion.

## ACKNOWLEDGMENTS

The authors thank Roi Baer, Mark Ratner, and Danny Neuhauser for extremely useful discussions as well as David Tannor, Efrat Rosenman, Anna Pomyalov, Jiří Vala, Guy Ashkenazi, and Vladimir Mandelshtam for sharing their views and comments. In particular, the authors are grateful to Hans-Joachim Freund for his continuing support. Volkhard May is acknowledged for careful reading of the manuscript. This work was supported in part by the German Israel Foundation GIF. The Fritz Haber Center is supported by the Minerva Gesellschaft für die Forschung, GmbH München, Germany.

- <sup>1</sup>J. Jortner and M. Bixon, (eds.) *Adv. Chem. Phys.* **106** (1999).
- <sup>2</sup>M. Bixon and J. Jortner, *Adv. Chem. Phys.* **106**, 35 (1999).
- <sup>3</sup>M. Bixon and J. Jortner, *Chem. Phys. Lett.* **159**, 17 (1989).
- <sup>4</sup>H. Guo, P. Saalfrank, and T. Seideman, *Prog. Surf. Sci.* **62**, 239 (1999).
- <sup>5</sup>T. Klüner, H.-J. Freund, V. Staemmler, and R. Kosloff, *Phys. Rev. Lett.* **80**, 5208 (1998).
- <sup>6</sup>R. A. Marcus, *J. Chem. Phys.* **24**, 966 (1956).
- <sup>7</sup>R. A. Marcus, *J. Chem. Phys.* **26**, 867 (1957).
- <sup>8</sup>G. Ashkenazi, R. Kosloff, and M. A. Ratner, *J. Am. Chem. Soc.* **121**, 3286 (1999).
- <sup>9</sup>O. V. Prezhdo, *Phys. Rev. Lett.* **85**, 4413 (2000).
- <sup>10</sup>P. F. Barbara, G. C. Walker, and T. P. Smith, *Science* **256**, 975 (1992).
- <sup>11</sup>P. Kambhampati, D. H. Son, T. W. Kee, and P. F. Barbara, *J. Phys. Chem. A* **104**, 10637 (2000).
- <sup>12</sup>R. Baer and R. Kosloff, *J. Chem. Phys.* **106**, 8862 (1997).
- <sup>13</sup>R. Baer, Y. Zeiri, and R. Kosloff, *Phys. Rev. B* **55**, 10952 (1997).
- <sup>14</sup>E. Geva, E. Rosenman, and D. Tannor, *J. Chem. Phys.* **113**, 1380 (2000).
- <sup>15</sup>U. Banin, A. Bartana, S. Ruhman, and R. Kosloff, *J. Chem. Phys.* **101**, 8461 (1994).
- <sup>16</sup>G. Ashkenazi, U. Banin, A. Bartana, R. Kosloff, and S. Ruhman, *Adv. Chem. Phys.* **100**, 229 (1997).
- <sup>17</sup>E. Geva, R. Kosloff, and J. L. Skinner, *J. Chem. Phys.* **102**, 8541 (1995).
- <sup>18</sup>D. H. Schirmer and V. May, *Chem. Phys. Lett.* **297**, 383 (1998).
- <sup>19</sup>C. Meier and D. J. Tannor, *J. Chem. Phys.* **111**, 3365 (1999).
- <sup>20</sup>R. Baer, Y. Zeiri, and R. Kosloff, *Surf. Sci.* **411**, L783 (1998).
- <sup>21</sup>N. V. Prokof'ev and P. C. E. Stamp, *Rep. Prog. Phys.* **63**, 669 (2000).
- <sup>22</sup>N. Makri, *Phys. Rev. B* **60**, 2823 (1999).
- <sup>23</sup>K. M. Forsythe and N. Makri, *Phys. Rev. B* **60**, 972 (1999).
- <sup>24</sup>A. A. Golosov, S. I. Tsonchev, P. Pechukas, and R. A. Friesner, *J. Chem. Phys.* **111**, 9918 (1999).
- <sup>25</sup>A. O. Caldeira, A. H. Castro Neto, and T. Oliveira de Carvalho, *Phys. Rev. B* **48**, 13974 (1993).
- <sup>26</sup>J. S. Bader and B. J. Berne, *J. Chem. Phys.* **100**, 8359 (1994).
- <sup>27</sup>R. Kosloff, *J. Phys. Chem.* **92**, 2087 (1988).
- <sup>28</sup>H. Tal-Ezer and R. Kosloff, *J. Chem. Phys.* **81**, 3967 (1984).
- <sup>29</sup>R. Kosloff, A. D. Hammerich, and D. Tannor, *Phys. Rev. Lett.* **69**, 2172 (1992).
- <sup>30</sup>E. Gershgoren, J. Vala, R. Kosloff, and S. Ruhman, *J. Phys. Chem. A* **105**, 5081 (2001).
- <sup>31</sup>L. W. Ungar and J. A. Cina, *Adv. Chem. Phys.* **100**, 171 (1997).
- <sup>32</sup>N. F. Scherer, R. J. Carlson, A. Matro, M. Du, A. J. Ruggiero, V. Romero-rochin, J. A. Cina, G. R. Fleming, and S. A. Rice, *J. Chem. Phys.* **95**, 1487 (1991).
- <sup>33</sup>S. Mukamel, *Principles of Nonlinear Optical Spectroscopy* (Oxford University Press, Oxford, 1995).
- <sup>34</sup>G. Ashkenazi, R. Kosloff, S. Ruhman, and H. Tal-Ezer, *J. Chem. Phys.* **103**, 10005 (1995).
- <sup>35</sup>R. Schanz, S. A. Kovalenko, V. Kharlanov, and N. P. Ernsting, *Appl. Phys. Lett.* **79**, 566 (2001).
- <sup>36</sup>M. R. Wall and D. Neuhauser, *J. Chem. Phys.* **102**, 8011 (1995).
- <sup>37</sup>J. W. Pang, T. Dieckmann, J. Feigon, and D. Neuhauser, *J. Chem. Phys.* **108**, 8360 (1998).
- <sup>38</sup>V. A. Mandelshtam and H. S. Taylor, *J. Chem. Phys.* **107**, 6756 (1997).
- <sup>39</sup>V. A. Mandelshtam, *J. Chem. Phys.* **108**, 9999 (1998).
- <sup>40</sup>E. P. Wigner, *Phys. Rev.* **40**, 749 (1934).
- <sup>41</sup>M. Hillery, R. F. O'Connell, M. O. Scully, and E. P. Wigner, *Phys. Rep.* **106**, 121 (1984).
- <sup>42</sup>I. S. Averbukh, M. J. J. Vrakking, D. M. Villeneuve, and A. Stolow, *Phys. Rev. Lett.* **77**, 3518 (1996).
- <sup>43</sup>D. M. Lockwood, M. Ratner, and R. Kosloff, *Chem. Phys.* **268**, 55 (2001).
- <sup>44</sup>V. May and O. Kühn, *Charge and Energy Transfer Dynamics in Molecular Systems* (Wiley-VCH, Berlin, 2000).
- <sup>45</sup>R. Kosloff and H. Tal-Ezer, *Chem. Phys. Lett.* **127**, 223 (1986).
- <sup>46</sup>T. Klüner, S. Thiel, and V. Staemmler, *J. Phys. B* **32**, 4931 (1999).
- <sup>47</sup>T. Pacher, L. S. Cederbaum, and H. Köppel, *Adv. Chem. Phys.* **84**, 293 (1993).
- <sup>48</sup>A. Kühl and W. Domcke, *Chem. Phys.* **259**, 227 (2000).
- <sup>49</sup>M. Topaler and N. Makri, *J. Phys. Chem.* **100**, 4430 (1996).
- <sup>50</sup>G.-L. Ingold and H. Grabert, "Sluggish decay of preparation effects in low temperature quantum systems," in *Quantum Probability and Applications V*, volume 1442 of *Lecture Notes in Mathematics*, edited by L. Accardi and W. von Waldenfels (Springer, New York, 1990), pp. 219–230.
- <sup>51</sup>G. Lindblad, *Commun. Math. Phys.* **48**, 119 (1976).
- <sup>52</sup>D. R. Yarkony, *J. Chem. Phys.* **114**, 2601 (2001).